Franklin Open 11 (2025) 100268

Contents lists available at ScienceDirect

Franklin Open

journal homepage: www.elsevier.com/locate/fraope

Developing a modelling environment of spacecraft solar array in low Earth orbit using real-time telemetry data

Ahmed Mokhtar [a], Mohamed Ibrahim [b,*], Mohamed E. Hanafy [a], Fawzy H. Amer ElTohamy [a], Yehia Z. Elhalwagy [c]

[a] Aircraft Electric Equipment Department, Military Technical College, Cairo, Egypt
[b] Automatic Control Systems Department, Military Technical College, Cairo, Egypt
[c] Vice Dean, Faculty of Engineering, Modern Sciences & Arts University (MSA), Giza, Egypt

ARTICLE INFO

Keywords:
Solar array
EPS system design
Low Earth orbit
Orbit illumination
Energy management and control

ABSTRACT

Spacecraft solar arrays convert sunlight into electrical energy to fulfil the energy requirements of various missions. This work proposes a comprehensive environment for accurate power operation predictions. Specifically, this environment simulates the behaviour of a body-mounted solar array. Furthermore, the designing and modelling processes of the solar array require considering different technical and practical constraints posed by the space environment. These challenges necessitate a thorough evaluation of all potential sources of losses and degradation. Compared to conventional approaches, our novel SSA model incorporates the complete spacecraft mission design scenario, thus it incorporates the operational cyclogram and power budget calculation. To substantiate our proposed method, telemetry data from the commercial LEOS-50 platform is leveraged to develop an experimental, mathematical, and thermal in-orbit model based on GaAs technology. This approach stands out for its exceptional accuracy in predicting the output power characteristics of solar panels. Therefore, it ensures achieving mission requirements from inception to completion in the beginning-of-life and end-of-life stages. The results demonstrate the success of the SSA operation in converting sunlight into electrical energy with a high conversion rate.

1. Introduction

Recently, several spacecraft in low Earth orbit (LEO) have played a crucial role in various fields, e.g., communication, weather monitoring, and scientific research. To achieve these missions, spacecraft solar arrays (SSA) convert sunlight into electrical energy to fulfil the energy requirements of all systems and instruments of spacecraft [1,2]. Unlike other conventional power sources, SSA provides a sustainable and renewable source of energy in space, where access to traditional energy sources is limited. Moreover, this electric power source, i.e., SSA, affects the design of the spacecraft mission and capabilities [3,4]. Developing a suitable SSA requires obtaining an accurate model to predict power operations and to simulate SSA behaviour to optimize spacecraft performance. This work proposes a systematic and comprehensive approach to ensure the proper functioning of micro-spacecraft in LEO orbits. This complete environment is used to simulate and design SSA that comprise body-mounted solar panels.

1.1. State of the art of SSA power modelling

In the literature, various modelling methods, e.g., mathematical and numerical models, as well as some simulation tools have been proposed. Generally, SSA models can be classified into analytical, numerical, and empirical approaches. Each method takes into account different factors, e.g., shading, efficiency, and output power. For instance, mathematical models based on physical principles are employed for predicting SSA performance. For example, the one-diode model and the Lambertian model allow to simulation of the electrical characteristics of solar cells. These models aid in predicting power output based on irradiance, temperature, and other variables. Otherwise, simulation and computational tools provide a virtual environment for analysing SSA performance by considering various environmental conditions and electrical characteristics. Software packages like MATLAB, PSpice, and PVsyst allow for simulating the SSA behaviour under different scenarios, e.g., shading effects. These tools greatly facilitate the design process leading to

* Corresponding author.
E-mail addresses: ahmed_refaie@ieee.org (A. Mokhtar), mohamed.ibrahim@mtc.edu.eg (M. Ibrahim), mehanafy@mtu.edu (M.E. Hanafy), ftha72@mtc.edu.eg (F.H.A. ElTohamy), y.elhalwagy@mtc.edu.eg (Y.Z. Elhalwagy).
URL: https://www.mtc.edu.eg/mtcwebsite/ (A. Mokhtar).

https://doi.org/10.1016/j.fraope.2025.100268
Received 19 November 2024; Received in revised form 20 March 2025; Accepted 20 April 2025
Available online 8 May 2025

improving the overall power generation efficiency and optimizing the array configurations. For a comprehensive review, the reader is referred to [5–10].

In the literature, several studies have addressed the power budgets analysis and design challenges of different CubeSat sizes (e.g., 1U, 2U, and 3U) with different power ranges [11–17]. For instance, [12] performed a power budget analysis method for a 1U CubeSat, considering operational modes and power consumption to determine the appropriate spacecraft configuration and battery capacity. The CubeSat power budget was analysed in [16] to determine the number of solar panels and batteries required for mission performance. The study calculated power requirements per orbit period, estimated power consumption, and calculated power generation by solar panels to inform the design of the power system. They also considered the utilization of previous solar panel designs to minimize development time and cost.

A reliable spacecraft power supply subsystem was designed in [18] based on discrete water cycle multi-objective optimization. Other studies [19,20] analysed the relationship between received solar irradiance and spacecraft orientation to optimize solar cell design and energy balance. However, some studies focused only on standby mode when analysing power consumption. Recent studies, e.g., [11], have explored power capacity requirements and EPS characteristics for LEO CubeSats in 5G applications. The study considered orbit altitude, coverage area, CubeSat movement, size constraints, volume resources, and 5G latency requirements. A mathematical and empirical model for a new spacecraft SSA power generation subsystem mission is designed and implemented [1,21].

In summary, these previous studies have explored power budget analysis, mission-specific power modes, and orientation scenarios for SSA design and validation. These considerations are crucial for efficient energy management in spacecraft missions with varying power requirements and design constraints.

1.2. Work contributions and structure

This work proposes a comprehensive environment for accurate power operation predictions. Specifically, this environment simulates and predicts the power operations of a body-mounted SSA to ensure the success of the micro-spacecraft mission. Furthermore, the proposed SSA model considers various technical and practical factors, e.g., the thermal effects, the degradation factors, and environmental conditions till the end of life (EOL) of the spacecraft. Compared to conventional approaches, our novel SSA model incorporates the complete mission design scenario, thus it incorporates the operational cyclogram and power budget calculation.

In this work, a mathematical and thermal in-orbit model is developed for Gallium Arsenide (GaAs) SSA, of 30% efficiency [22] using the telemetry data of a commercial LEOS-50 platform [23]. This developed model verifies the capability of the LEOS-50 platform [23], to execute the proposed power budget. Therefore, it ensures achieving mission requirements from inception to completion at both the beginning-of-life and end-of-life stages. To maximize power generation, we consider various design factors, e.g., orientation, orbital dynamics, interconnection, arrangement of solar cells, and deployment mechanisms.

This paper is organized as follows: The SSA model, equivalent circuit, and power budget calculations are represented in Section 2. Mission cyclogram design scenarios with power budget calculations are described in Section 4. The simulation results are discussed in Section 6. Section 7 concludes the proposed work.

2. Spacecraft solar array model

The SSA is a crucial component of space missions that consists of multiple interconnected solar panels, which convert sunlight into electrical energy to power various systems on the spacecraft. The first step in designing and analysing spacecraft power systems is to obtain an accurate SSA model to optimize performance and ensure mission success. This model should incorporate various design aspects, e.g., panel dimensions, deployment mechanisms, material properties, incident solar flux, and orientation relative to the Sun to maximize energy production while withstanding the harsh conditions of outer space.

2.1. Factors affecting SSA performance in LEO orbit

Practically, SSA efficiency in LEO orbit is influenced by various factors, e.g., variations in sunlight intensity, orbital dynamics, and microgravity conditions. For instance, the sunlight intensity varies in LEO due to Earth atmosphere, Sun angle, and orbital position. Therefore, the arrangement of solar cells in an SSA system is crucial for maximizing power generation. Additionally, deployment mechanisms are carefully constructed to ensure the seamless unfolding of the arrays after launch.

Therefore, orbiting around the Earth should be considered to maximize power generation by optimizing the spacecraft orientation. For instance, solar irradiance variations directly impact power generation capabilities. Moreover, spacecraft orientation and eclipse shadowing reduce the SSA exposure to sunlight. Orientation scenarios and their impact on spacecraft performance and power generation were investigated in various papers, e.g., [19,20]. Moreover, ballistic and dynamic calculations of the spacecraft route are performed. Power budgeting also takes into account the spacecraft orbit and orientation to balance the coverage area and power generation requirements of the radio communication subsystem [11,17]. Therefore, SSA configurations should be designed to minimize shadowing to ensure consistent power generation. On the other hand, SSA can experience significant temperature fluctuations, which affect their electrical performance and lifespan. To mitigate these effects, thermal insulation and heat dissipation mechanisms must be carefully considered to ensure optimal power generation.

Efficiency and conversion rates are the main factors of solar power generation in space. For instance, the degradation and ageing of any solar cell affect the SSA performance. Hence, degradation and ageing cause challenges to maintaining optimal power continuously [5].

Practically, SSA designing and modelling face various challenges and uncertainties for LEO spacecraft due to limited resources. Moreover, there are always technical and practical constraints that should be considered to develop the perfect SSA model. For instance, computational complexity and real-world testing and validation should be taken into account for space applications. Recently, as technology continues to advance, addressing the challenges and limitations in SSA modelling has become imperative for LEO spacecraft. By continuously refining our modelling approaches and exploring innovative solutions, we can enhance the power generation capabilities of SSAs [23–25].

2.2. Optimizing SSA design for LEO spacecraft

The required power and regulated voltage should be achieved during SSA design to successfully provide continuous and conditioned power to various loads of the spacecraft. Practically, SSA manufacturing requires careful consideration of various factors, e.g., advanced technologies, architecture, and structural configuration [19].

Recently, various manufacturing techniques have been proposed to enhance solar cell performance and efficiency to maximize the generated power. For instance, modern technology and innovative approaches have been utilized using new materials to squeeze every last drop of power from these tiny solar cells. Moreover, it is important to develop innovative approaches for designing lightweight and compact SSA as every gram counts in space. For instance, different types of SSA have been produced recently, e.g., monocrystalline, polycrystalline, and thin-film, each has its characteristics, e.g., efficiency, weight, and cost. Therefore, selecting the right SSA technology for LEO spacecraft

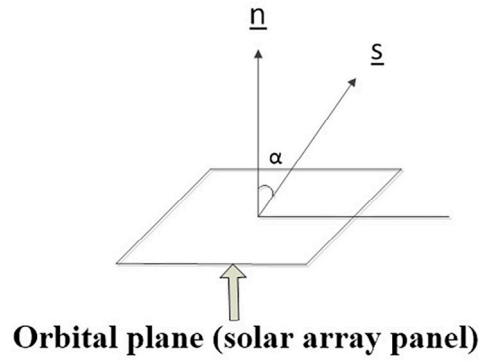

Fig. 1. Angle (α) between the normal to an orbital plane and Sun direction.

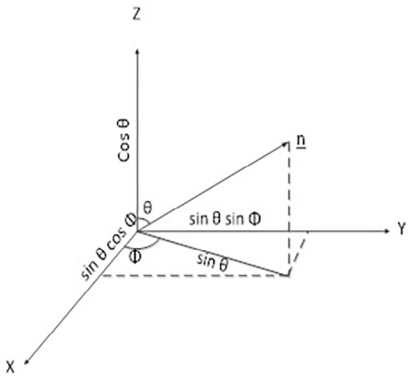

Fig. 2. Projection of vector (n) in BCS.

involves striking a balance between power generation and mass and space constraints as well as reliability [7,8] .

By understanding the design principles, we can optimize the efficiency and reliability of SSA utilizing advanced modelling techniques considering the various factors impacting performance. SSA structures must maintain the desired power output while enduring the harsh conditions of space, e.g., extreme temperatures, radiation, and micrometeoroids. The key aspects of SSA structural design include materials selection and deployment mechanisms as well as mechanical stability. This article explores the modelling techniques of SSA power generation for LEO spacecraft [9,26] .

2.3. Mathematical and computational equations

The SSA model uses mathematical equations and computational methods to simulate the electrical characteristics of the SSA, e.g., voltage output and current generation in different operational conditions. These outputs are used to evaluate energy conversion efficiency, optimize deployment strategies, assess thermal effects on performance, and identify potential structural issues.

In this context, the SSA output power depends on the SAA type, orbital parameters, the SSA orientation, and illumination conditions as well as thermal parameters. Moreover, the SSA output power depends on air mass zero $AM0 = 1370$ [W/m^2], which is the total solar energy incident on a unit area perpendicular to the sun's rays at the mean earth–Sun distance on top of the earth's atmosphere. The illumination Coefficient K_{ill} is expressed in (1) for the spacecraft panels according to the angle [α] of each face of the spacecraft (body mounted configuration) as shown in Fig. 1.

$$K_{ill} = \underline{n} \odot \underline{S} = n * S \cos\alpha \tag{1}$$

From dot product in Eq. (1) since vector n, S are a unit vector then $|\underline{n}|, |\underline{S}| = 1$ and the illumination factor can be calculated as [27–29].

$$\cos\alpha = \underline{n} \odot \underline{S} = \text{ illumination coefficient }, \tag{2}$$

Where $\underline{n}$ is the normal vector to the SSA plane, and $\underline{S}$ is the direction to the Sun vector.

Calculation of normal vector (n)

The calculation of the projection of $\underline{n}$ in the body coordinate system (BCS) is shown in Fig. 2. The vector $\underline{n}$ is expressed as

$$\underline{n} = \sin(\theta)\cos(\phi)\underline{x} + \sin(\theta)\sin(\phi)\underline{y} + \cos(\theta)\underline{z}, \tag{3}$$

Here, ϕ is the angle between the X axis and the projection of the vector n in the XY plane. θ is the angle between the Z-axis and vector n.

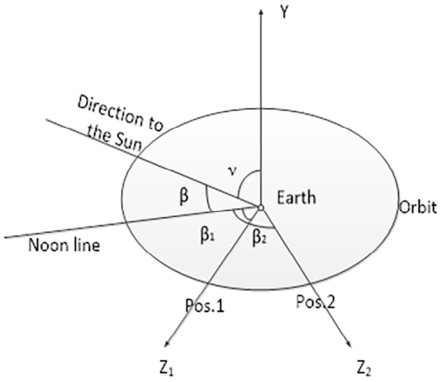

Fig. 3. Calculation of vector (S) by using OCS.

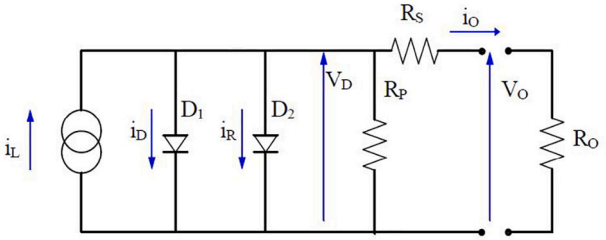

Fig. 4. Equivalent circuit of PVC.

Calculation of vector (s)

Using the orbital coordinate system (OCS) as shown in Fig. 3, the vector (S) is expressed as

$$\underline{S} = -\sin(\nu)\sin(\beta)\underline{z_1} + \cos(\nu)\underline{z_2} + \sin(\nu)\cos(\beta)\underline{Y} \tag{4}$$

Where β is the angular position of the spacecraft in orbit (in shadow or the sun) at any instant, ν is the angle between the direction to the Sun and the normal to the orbital plane. The optimal Sun vector is obtained using the illumination modal orientations of the spacecraft faces during the worst-case scenario. The optimum Sun vector is calculated to achieve optimum illumination of the spacecraft faces as

$$(1/\sqrt{11}, -3/\sqrt{11}, -1/\sqrt{11})$$

2.4. Solar cell equivalent circuit

The equivalent circuit of a spacecraft solar cell simplifies the complex physical processes occurring within the solar cell, enabling precise analysis and characterization of its electrical behaviour and optimizing

its operation. The equivalent circuit, see Fig. 4, consists of p–n junction diodes and resistors as well as photovoltaic current sources driven by the voltage value applied at its terminals. These components represent essential phenomena, e.g., carrier recombination, diffusion current, series resistance losses, and shunt resistance losses. Quantifying these parameters accurately leads to maximizing efficiency and reliability in space missions.

Generally, a solar cell, or a photovoltaic cell (PVC), is a particular p–n junction. In this junction, the diffusion process (diode D1) co-exists with the generation and recombination effect of the charge carrier (diode D2) induced by the presence of crystalline defects. This model is for a triple-junction solar cell with an efficiency of (30%), which has been tested and validated by the manufacturer (AZUR SPACE company) and is available on the company website [22] . The mathematical model of PVC should consider the intensity of the incident light, operational temperature, and degradation due to the space radiation [27–29]. In the same context, the electrical properties of GaAs solar cells, e.g., their high efficiency and temperature stability, influence the equivalent circuit model. For example, the high open-circuit voltage (V_{oc}) and low temperature coefficient of GaAs cells are incorporated into the diode equations used in the model:

$$I_{\text{solar cell}} = I_{SC} - I_S \times (e^{r(V+I\cdot R_s)} - 1),$$

where I_{SC} is the short-circuit current, I_S is the reverse saturation current, and R_s is the series resistance.

2.5. Solar array mathematical model

The SSA mathematical model depends on the PVC characteristics [22,30] . The volt–ampere characteristic (VAC) equation is given by:

$$I_{\text{solar cell}} = I_{SC} - I_S \times \left(e^{\gamma(V+(rI))} - 1\right), \tag{5}$$

Where I_S [A] is reverse saturation current, γ is the VAC shape factor, $r[\Omega]$ is PVC series resistance, I [A] is the PVC load current, V [V] is the PVC load voltage. I_{sc} [A] is the short circuit current of the solar cell, it can be equal to the PVC short circuit current I_o is given the low difference of values between them.

Using the values of short circuit current I_o, open circuit voltage V_{oc}, current and voltage at maximum point I_m and V_m, given in Table 5, the values of r, γ and I_s can be calculated as follows:

$$r = \frac{V_m}{I_m} - \frac{1}{\gamma \times \left(I_{0-I_m}\right)} \tag{6}$$

$$\gamma = \frac{\frac{I_m}{I_0-I_m} + \ln\left(1 - \frac{I_m}{I_0}\right)}{2 \times V_m - V_{\Omega c}} \tag{7}$$

$$I_s = \frac{I_0}{e^{\gamma \times V_{oc}-1}} \tag{8}$$

The output electric power given by PVC is given by:

$$\mathbf{P} = \mathbf{V} \cdot \mathbf{I} \tag{9}$$

This mathematical model reflects the specific performance characteristics of GaAs solar cells, e.g. their high conversion efficiency (30%) and low degradation rate. This includes the calculation of maximum power point (P_m) and the impact of GaAs's superior radiation resistance on long-term performance.

2.6. Solar array power budget calculation

The SSA power budget calculation is an essential process in the spacecraft design and operation. It involves determining and optimizing the available power generated by the SSA for all mission phases without experiencing any energy shortage or interruption. The objective is to ensure that enough power is generated and stored in batteries during the orbital day to meet all energy demands during orbiting daylight and eclipse periods. This calculation takes into account various factors, e.g., the cell efficiency, their degradation over time, and eclipse periods. In this section, the whole calculation of the SSA generated power is consistent with the methodology obtained by previous works [11,31].

2.6.1. Solar cell-specific output power calculation

The specific output power determines the efficiency and effectiveness of the solar cells in converting sunlight into electrical energy to power various spacecraft subsystems. To calculate this value, several factors must be considered, e.g., incident solar radiation, eclipse periods, orientation angles, and solar cell characteristics, such as area, efficiency, and temperature coefficient. All these variables are then used in complex mathematical equations to determine the specific output power for each solar cell and consequently assess its contribution to overall power generation.

Assuming that the Sun radiation is normal to the cell surface, the specific output power $P_{o/TJ}$ [W/m^2] is expressed as:

$$P_{o/TJ} = \text{AM}_0 \times \eta_{TJ} = 1370 \times 0.3 = 410.1\ \left[\text{W/m}^2\right], \tag{10}$$

Where η_{TJ}: efficiency of Triple junction solar cells which is assumed to be 30%.

2.6.2. Performance degradation models

This subsection outlines the factors contributing to solar array degradation, including radiation exposure, temperature effects, and system efficiency losses.

Degradation coefficient calculation

Degradation coefficient calculation plays a vital role in determining SSA performance and longevity. This calculation considers various factors, e.g., the radiation environment such as proton and electron fluxes, as well as the thickness and composition of protective covers on the solar cells. Practically, the degradation rate depends on multiple parameters, e.g., cell technology and quality, mission orbit, and shielding design. These factors affect the $I - V$ characteristic of the SA. By employing advanced modelling techniques using data from previous missions, professionals can accurately estimate cell-degradation coefficients, aiding in reliable spacecraft system design and operation. In general, the calculation considers both short-term and long-term degradation to predict the overall decline in cell efficiency over time. The average degradation coefficient K_d is defined as the factor by which the solar cell's efficiency decreases over time due to space radiation and other environmental factors. It is calculated using the following equation [1,21]:

$$K_d = \left[1 - \left(D_{\text{TJ}}\right)\right]^{Sat_L} = \left[1 - \left(\frac{2}{100}\right)\right]^2 = 0.9604, \tag{11}$$

where D_{TJ} is the degradation coefficient of triple-junction solar cells, representing the annual percentage decrease in efficiency due to the influence of the space environment. For this study, D_{TJ} is assumed to be 2% per year, based on empirical data from previous missions using GaAs solar cells in LEO orbit. This coefficient accounts for the cumulative effects of radiation, temperature cycling, and other environmental factors. Sat_L is the spacecraft's lifetime in years (assumed to be 2 years). This equation accounts for the cumulative effect of degradation over the mission duration.

Specific output power degradation due to system efficiency

Over time, the solar cells experience degradation in their specific output power due to system efficiency, radiation damage, temperature effects, and production defects. Therefore calculating the specific actual power, $P_{act/TJ}$ [W/m^2], takes into account the system efficiency , η_{sys}, including wire losses, chemical battery, blocking diodes, etc [1,21].

$$P_{act/TJ} = P_{t/TJ} \times \eta_{\text{sys}} \tag{12}$$

Assuming a system efficiency $\eta_{sys} = 0.9$, which accounts for losses due to wiring, blocking diodes, battery charging/discharging inefficiencies, and other parasitic losses in the power distribution system. This value is based on empirical data from similar spacecraft power systems and is consistent with industry standards for LEO missions.[1] Therefore, $P_{act/TJ} = 348.054 \times 0.9 = 313.25$ [W/m^2]. So understanding and mitigating these degradation mechanisms is crucial for maintaining maximum power generation from spacecraft solar cells and ensuring optimal performance throughout their operational lifespan.

2.6.3. EOL specific output power calculation

With a finite lifespan, solar cells experience degradation over time due to factors, e.g., radiation exposure and temperature fluctuations. Calculating the specific output power at end-of-life (EOL) must consider various factors, e.g., the initial rated output power, degradation rate, and estimated lifetime. By accounting for these factors, the EOL-specific output power can be estimated using empirical or analytical models based on prior space mission data. The EOL specific output power, $P_{O/EOL}$ [W/m^2] is given by:

$$P_{O/EOL} = P_{o/TJ} \times K_d \tag{13}$$
$$P_{O/EOL} = 410.1 \times 0.9604 = 393.86 \left[\mathrm{W/m^2}\right]$$

This calculation allows evaluation of whether anticipated energy will meet operational requirements throughout its intended lifespan or if necessary mitigating strategies need to be implemented to maintain optimum performance.

2.6.4. Temperature coefficient calculation

Solar cells are sensitive to temperature variations significantly affecting their power output. Practically, the SSA is exposed to a wide range of temperatures during its operation under space environmental conditions. Therefore, temperature coefficient calculation considers various factors, e.g., temperature coefficients of voltage, current, power, and efficiency. These values are usually obtained through extensive testing under controlled conditions. Accurate calculations of the temperature coefficient ensure that the cells can deliver optimal performance regardless of the harsh conditions in space. For instance, if the spacecraft is in the shadow period, the SSA temperature can get as low as −80 °C. The highest operating temperature for the SSA of the spacecraft under study is 70 °C, occurring during the sunlit period. These temperature variations affect the I-V characteristic of the SA. Therefore, a temperature coefficient K_t must be taken into account [1,21]:

$$K_t = (1 + \epsilon \times \Delta \mathrm{T}) \tag{14}$$
$$\Delta \mathrm{T} = T_{\max} - T_{\mathrm{ambient}} = 70 - 28 = 42\ ^\circ\mathrm{C} \tag{15}$$

Where K_t: Temperature coefficient, $T_{\max}$: Maximum temperature = 70 °C, for altitude = 668 km, T_{ambient} = 28 °C, $\epsilon = -0.0025\ ^\circ\mathrm{C}^{-1}$, The temperature coefficient of the triple junction solar cell degrades the output power ($P_{(O/EOL)}$), so $K_t = 0.89$. The specific output power at regulation temperature, $P_{t/TJ}$ [W/m^2] can be calculated as follow [1, 21]:

$$P_{t/TJ} = P_{O/EOL} \times K_t \tag{16}$$
$$= 393.86 \times 0.89 = 348.054 \left[\mathrm{W/m^2}\right]$$

[1] The assumed system efficiency is validated using real-time telemetry data from the LEOS-50 platform, which operates under similar conditions. The power generation and distribution performance of the platform align with the assumed efficiency, supporting the use of $\eta_{sys} = 0.9$ in the model.

2.6.5. Effect of illumination coefficient on output power calculation

Calculating the illumination coefficient is a crucial aspect in the design and operation of spacecraft to optimize energy generation and ensure an uninterrupted power supply during missions. Practically, the solar radiation flux density (illumination) affects the electrical power characteristics of the SSA during its operation under space environmental conditions [30]. Thus this coefficient represents the time fraction that a solar cell receives direct sunlight, determining its efficiency and power output. Estimating this coefficient includes various factors, e.g., spacecraft trajectory, Earth obliquity, shadowing effects, and atmospheric interference.

In this context, the specific output power depends on the change of illumination angle on the SSA and the illumination of the orbit. The specific output power P_{ill} [W/m^2] of a triple-junction (TJ) solar array considering system efficiency losses is expressed as [30]:

$$P_{\mathrm{act/TJ}} = P_{t/TJ} \times \eta_{\mathrm{sys}} \tag{17}$$

where $P_{\mathrm{act/TJ}}$ [W/m^2] is the actual specific output power of the solar array after accounting for system losses. $P_{t/TJ}$ [W/m^2] is the specific output power of the TJ solar cell at the operating temperature. η_{sys} (dimensionless, range: 0–1) is the system efficiency, which accounts for losses in power conditioning, wiring, and battery charging.

The nominal specific power output of a TJ solar cell is influenced by factors such as radiation degradation, thermal effects, and system aging. The power at the operating temperature is given by:

$$P_{t/TJ} = P_{O/EOL} \times K_t \tag{18}$$

where $P_{O/EOL}$ [W/m^2] is the specific power at the end-of-life (EOL), considering radiation and aging effects. K_t (dimensionless) is the temperature correction factor, accounting for power reduction due to temperature variations.

The system efficiency factor (η_{sys}) accounts for losses occurring in the electrical power system, including:

- Power conversion losses in regulators and converters.
- Resistive losses in wiring and connections.
- Blocking diode and switch losses.
- Energy conversion inefficiencies in battery charging and discharging.

The overall system efficiency is expressed as:

$$\eta_{\mathrm{sys}} = \eta_{\mathrm{wiring}} \times \eta_{\mathrm{conversion}} \times \eta_{\mathrm{battery}} \tag{19}$$

where η_{wiring} represents efficiency losses in power distribution wiring. $\eta_{\mathrm{conversion}}$ accounts for DC-DC converter efficiency. η_{battery} considers battery charge/discharge efficiency. For this study, assuming typical values $\eta_{\mathrm{sys}} = 0.9$ which corresponds to a 90% overall system efficiency. The final computation is obtained by substituting realistic values as:

$$P_{t/TJ} = 348.05\ \mathrm{W/m^2}, \quad \eta_{\mathrm{sys}} = 0.90$$
$$P_{\mathrm{act/TJ}} = 348.05 \times 0.90 = 313.25\ \mathrm{W/m^2}$$

After accounting for power conversion and system losses, the actual available power for the spacecraft is 313.25 W/m^2. Eq. (17) provides a quantitative relationship for estimating the real-world power output of spacecraft solar arrays after accounting for environmental and system losses. This equation is essential for designing power budgets and ensuring adequate energy supply for mission operations.

The power budget calculations explicitly consider the properties of GaAs technology, e.g. the higher specific power output ($P_{o/TJ}$) and lower degradation coefficient (K_d). For example:

$$P_{o/TJ} = AM0 \times \eta_{TJ} = 1370 \times 0.3 = 410.1\ \ [\mathrm{W/m^2}],$$

where η_{TJ} is the efficiency of the triple-junction GaAs solar cell. The temperature Correction Factor K_t is given by:

$$K_t = (1 + \epsilon \times \Delta T) \tag{20}$$

where ϵ [1/K] is the temperature coefficient of the solar cells, representing the rate at which power output decreases per degree rise in temperature. ΔT [K] is the temperature variation, calculated as:

$$\Delta T = T_{\max} - T_{\text{ambient}} \tag{21}$$

where $T_{\max}$ [K] is the maximum expected operating temperature of the solar array. T_{ambient} [K] is the reference ambient temperature in space. Using assumed values:

$$T_{\max} = 70\ ^\circ\text{C}, \quad T_{\text{ambient}} = 28\ ^\circ\text{C}, \quad \epsilon = -0.0025\ \text{K}^{-1}$$
$$\Delta T = 70 - 28 = 42\ \text{K}$$
$$K_t = 1 + (-0.0025 \times 42) = 0.89$$

Substituting into Eq. (18)

$$P_{t/TJ} = 393.86 \times 0.89 = 348.05\ \text{W/m}^2$$

The system efficiency factor accounts for power losses in the electrical system, such as wiring resistance, conversion inefficiencies, and battery charge/discharge losses.

$$\eta_{\text{sys}} = \eta_{\text{wiring}} \times \eta_{\text{conversion}} \times \eta_{\text{battery}} \tag{22}$$

where η_{sys} (dimensionless) is the overall system efficiency, which determines how much of the generated power is effectively available for spacecraft systems. η_{wiring} (dimensionless) represents losses in power distribution wiring due to resistance (0.98 typical value). $\eta_{\text{conversion}}$ (dimensionless) accounts for DC-DC converter efficiency, typically around 0.95. η_{battery} (dimensionless) represents efficiency losses during battery charging and discharging, usually around 0.97. Using realistic values:

$$\eta_{\text{sys}} = 0.98 \times 0.95 \times 0.97 = 0.90$$

Substituting values into Eq. (17):

$$P_{\text{act/TJ}} = 348.05 \times 0.90 = 313.25\ \text{W/m}^2$$

Eqs. (18) and (19) provide essential corrections for estimating real-world power availability from spacecraft solar arrays. Eq. (18) adjusts for temperature effects, while Eq. (19) accounts for system losses, ensuring accurate power budgeting.

Practically, the GaAs technology enhances the solar array's performance in LEO. This includes:

- High Efficiency: GaAs solar cells have a higher conversion efficiency compared to traditional silicon-based cells, resulting in greater power generation per unit area.
- Radiation Resistance: GaAs cells are more resistant to radiation-induced degradation, which is critical for maintaining performance over the spacecraft's mission lifetime.
- Temperature Stability: The low temperature coefficient of GaAs cells ensures stable performance under the extreme temperature variations encountered in LEO.

2.7. Solar array area calculation

The solar panels on a spacecraft are crucial for capturing sunlight and converting it into electrical energy to power various onboard systems. Therefore, calculating the SSA area is an integral part of spacecraft design to ensure optimal power generation while minimizing weight and costs. Calculating the SSA area requires considering factors, e.g., power requirements, expected sunlight exposure, orbital parameters, eclipse duration, and solar panel efficiency. These calculations involve advanced mathematical models using state-of-the-art simulation tools and computer algorithms.

Based on these calculations, the required area of the solar array, S_{sa} [m^2] is expressed as:

$$S_{sa} = \frac{P_{\text{daily/avg}}}{P_{\text{act }/TJ}} = \frac{35}{95.892} = 0.36\ \text{m}^2 \tag{23}$$

$$\begin{aligned} S_{\text{sa/act}} &= S_{sa} \times \text{ safety and packing factor} \\ &= 0.36 \times 1.1 = 0.4\ [\text{m}^2] \end{aligned} \tag{24}$$

2.8. Chemical battery model and operating conditions

This section discusses the operating conditions of chemical batteries, including temperature variations, charge/discharge cycles, and the impact of orbital dynamics on battery performance. Moreover, this section outlines the mathematical formulation of the chemical battery model, including equations for battery capacity, discharge characteristics, and energy storage.

2.8.1. Chemical battery sizing

The chemical batteries serve as the primary power source for spacecraft, providing electricity during eclipse periods. Therefore, the proper size of the spacecraft chemical battery is an essential aspect of spacecraft design to ensure uninterrupted operation. On another hand, it is required to optimize spacecraft structure fulfilling cost, weight, and volume constraints, allowing for efficient allocation of resources while guaranteeing long-term energy functionality. Determining the proper size requires considering various factors, e.g., mission duration, power consumption, and worst-case scenarios. Additionally, the thermal management system is required to maintain appropriate battery temperatures and prevent overheating or freezing during extreme temperature variations in space. In chemical battery sizing, the required battery capacity is determined, and then its mass is calculated.

It is necessary to consider the operating conditions of chemical batteries, including temperature variations, charge/discharge cycles, and the impact of orbital dynamics on battery performance. This includes:

- Temperature Effects: The influence of extreme temperature fluctuations in LEO on battery efficiency and lifespan.
- Eclipse Periods: The role of chemical batteries in providing power during eclipse periods, including the calculation of energy requirements and battery sizing.
- Mission Constraints: The integration of battery operating conditions with mission-specific requirements, such as power consumption profiles and mission duration.

2.8.2. Chemical battery capacity calculation

The chemical batteries are vital elements in the spacecraft that facilitate power generation during eclipse phases or backup power during emergencies. Therefore calculating the capacity of the chemical battery is a crucial task in the aerospace industry that involves assessing the energy storage capabilities of the battery system. Furthermore, accurate estimation is essential to ensure uninterrupted power supply throughout a spacecraft entire operational life cycle.

These calculations require mathematical models and simulations using extensive empirical data considering various factors, e.g., environmental conditions like temperature variations, and discharge rates that impact the durability and lifespan of the battery. Moreover, it is important to calculate the average and peak power demands of each onboard system. Furthermore, precise calculation knowledge of specific spacecraft technologies and battery chemistry.

In this work, the calculation of the chemical battery capacity is based on various data:

- The daily average power consumption $\text{P}_{\text{dailv/avg}} = 35$ W.
- The efficiency of the lithium iron phosphate chemical battery $\eta_b = 0.8$,
- Average bus voltage $V_{avg} = 28$ V,
- Energy density for lithium iron chemical batteries $E_d = 157$ Wh/kg.

The energy consumed during the orbital shadowed period (E_{Shadow}) is expressed as [1,2]:

$$E_{\text{Shadow}} = \frac{P_{\text{daily/average}} \times T_{\text{Shadow}}}{\eta_b}, \tag{25}$$

Where E_{Shadow} is the energy consumed during the shadow period [Wh], and shadow time is 31.05 min calculated from STK simulation for the spacecraft in orbit as a worst-case shadow time.

$$E_{\text{Shadow}} = \frac{35 \times \frac{31.05}{60}}{0.8} = 22.640 \text{ Wh}$$

The energy consumed during the shadow period can be expressed by ampere-hour:

$$E'_{\text{Shadow}} = \frac{E_{\text{Shadow}}}{V_{\text{avg}}} = \frac{22.640}{23.5} = 0.9634 \text{ Ah} \quad (26)$$

The required depth of discharge $DOD = 20\%$ is specified to preserve the battery efficient operation during the spacecraft lifetime. The battery-rated capacity (C_{rated}) is expressed as:-

$$\text{C}_{\text{rated}} = \frac{\text{E}'_{\text{shadow}}}{\text{DOD}} = \frac{0.9634}{0.2} = 4.817 \text{ Ah} \quad (27)$$

2.9. SSA ray direction tracking model

The SSA efficiency is a crucial factor in mission success as it provides the primary power source for onboard systems. The efficiency of an SSA depends on its ability to maintain alignment with the Sun's rays [32]. Therefore, it is required to ensure optimal orientation of the SSA relative to the Sun using an efficient sun-tracking mechanism.

2.9.1. Sun-tracking mechanisms

To achieve this, spacecraft employ various sun-tracking mechanisms, which can be classified as:

- **Fixed solar arrays:** Passive solar arrays fixed to the spacecraft body, requiring attitude control maneuvers for optimization.
- **Active sun-tracking systems:** Mechanically actuated systems that dynamically orient the solar arrays.

Active tracking is superior, as it continuously maximizes energy collection [33].

2.9.2. Solar Array Drive Assemblies (SADAs)

Solar Array Drive Assemblies (SADAs) are electromechanical systems that rotate SSA to track the Sun's movement. These systems can be classified into:

- **Single-axis SADAs:** Allow rotation around one axis, typically suitable for geostationary satellites.
- **Dual-axis SADAs:** Enable movement along two perpendicular axes, allowing finer Sun tracking in low-Earth orbits.

The torque disturbances caused by SADAs must be minimized to prevent affecting spacecraft attitude stability [34].

2.9.3. Modelling sun-tracking behaviour

The ray direction tracking model governs the SSA alignment with the Sun to maintain optimal energy generation throughout the mission. The SSA orientation is governed by their normal vector relative to the Sun's direction:

$$\theta = \cos^{-1}(\hat{n} \cdot \hat{S}), \quad (28)$$

where θ is the Sun incidence angle, $\hat{n}$ is the unit normal vector to the SSA, $\hat{S}$ is the unit vector pointing towards the Sun. Minimizing θ ensures optimal energy absorption. Sun sensors and onboard algorithms dynamically adjust $\hat{n}$ to track the Sun efficiently [35].

Implementing sun-tracking systems involves several challenges, e.g., mechanical complexity, control algorithms, and disturbance mitigation. Recent advancements in SSA tracking include flexible SSA [36], machine learning-based tracking [35] miniaturized SADAs [34]. The ray direction tracking model is a fundamental aspect of spacecraft power management. By integrating SADAs, analytical models, and advanced control strategies, spacecraft can ensure optimal solar energy collection.

2.10. External thermal fluxes

In LEO, the incoming solar radiation varies due to factors, e.g., changing orbital positions, eclipse events, and orientation variations. These fluctuations significantly impact the overall thermal balance of the solar array and, thus, its efficiency. Therefore, it is important to assess and analyse these external thermal fluxes to accurately predict temperature levels and mitigate any potential issues, e.g., degradation or failure of photovoltaic cells.

To ensure proper design, advanced modelling techniques have been employed using real data accounting for these external thermal fluxes on solar arrays of LEO spacecraft. So, calculating the external fluxes is very important to estimate the real generated power from SSA during the real operation. Estimating the dynamic behaviour of the SSA power requires the instantaneous calculation of the three absorbed thermal fluxes with the true anomaly in orbit. These fluxes include the thermal flux of direct solar radiation, Q_S, the thermal flux of reflected solar radiation, Q_{SO}, and the thermal flux of Earth radiation, Q_Z.

In this work, a separate module is implemented to estimate the whole thermal fluxes as represented:

$$\text{Q}_\text{i} = \text{Q}_\text{S} + \text{Q}_\text{SO} + \text{Q}_\text{Z} + \text{Q}_\text{K} \quad (29)$$

where Q_S thermal flux of direct solar radiation, (W/m^2). Q_{SO} is thermal flux of reflected solar radiation, (W/m^2). Q_Z thermal flux of Earth radiation, (W/m^2). Q_K thermal flux between two surfaces of SA, (W/m^2).

$$\text{Q}_\text{ss} = \text{a}_\text{ss} \times \text{S}_\text{o} \times \cos\alpha_\text{j} \quad (30)$$

Where a_{ss} is the irradiation absorption factor of the work surface = 0.886. S_0 is the average solar irradiance constant, considered as AM0 = 1370 [W/m^2]. α is the angular position. The value of thermal fluxes is represented as

$$\text{Q}_\text{ss} = 1204.5 \times \cos\alpha_{\text{j}_2} \left[\text{W/m}^2\right],$$
$$\text{Q}_\text{so} = 231.29 \times \cos\alpha_i, \left[\text{W/m}^2\right]$$

$Q_Z = 140$, [W/m^2], "Q_K, the thermal flux between two surfaces of the solar array, is neglected in this analysis because its contribution is negligible compared to the dominant thermal fluxes Q_S, Q_{SO}, and Q_Z. This assumption is justified by the relatively small temperature differences between the solar array surfaces and the minimal heat exchange between them in the space environment.

Fig. 5 represents the simulation result of the external fluxes absorbed Q_i VS true anomaly β during the operation of the SSA in orbit with all external factors. The flux components are decomposed into their primary contributors:

1. S0S0: The average solar irradiance constant, presented as the baseline contribution from solar radiation in space, measured in W/m^2.
2. QSQS: The thermal flux of direct solar radiation, demonstrating the periodic exposure of the solar arrays to sunlight as the spacecraft moves along its orbit.
3. QSOQSO: The thermal flux of reflected solar radiation, accounting for the contributions from Earth albedo effects.
4. QZQZ: The thermal flux of Earth radiation, representing the thermal emission from Earth surface and atmosphere.

Fig. 5 captures the periodic nature of these fluxes, driven by the spacecraft dynamics and its orientation concerning the Sun and Earth. Peaks correspond to periods of direct exposure to sunlight, while dips indicate eclipse phases where the spacecraft is shielded from solar radiation. The comparative magnitudes of QSQS, QSOQSO, and QZQZ highlight the dominance of direct solar radiation (QSQS) in determining the external thermal environment of the solar arrays. This visualization validates the modelling environment designed for simulating spacecraft SSA performance in LEO, as detailed in the study.

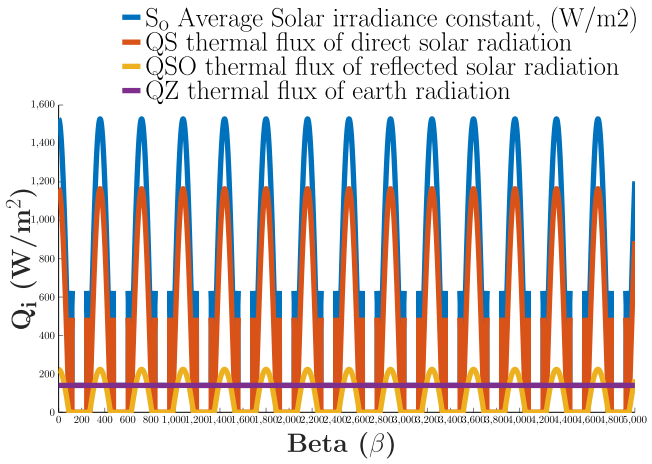

Fig. 5. Variation of external thermal fluxes as a function of the true anomaly β, representing the angular position of the spacecraft relative to the Sun.

The real-time telemetry data used for model calibration ensures the accuracy of these flux predictions under actual operational conditions, underscoring the model's capability to capture the intricate thermal dynamics encountered in space.

2.11. The thermal balance of the solar array

Practically, the thermal balance of the SSA is crucial to maximize the energy conversion efficiency for successful spacecraft operation. It should also ensure the SSA capability to withstand space environmental conditions. Both heat dissipation and insulation should be taken into account to maintain optimal performance and prevent any damage due to extreme temperature variations. Additionally, efficient heat transfer mechanisms might be employed to dissipate excess heat. The design should account also for the spacecraft's position towards the Sun and shadowing effects from other components. In this work, a model of thermal balance and temperature calculation is implemented. The thermal balance model includes the thermal coefficient $\epsilon = 0.0025[1/\text{degree}]$, which quantifies the reduction in specific power due to temperature variations. This coefficient is used to calculate the change in specific power as follows:

$$\Delta T \quad = T1 - To; To = 298\ [K^{\circ}] \tag{31}$$

Reduction of SSA-specific power due to thermal effects:

$$P_{th} = P_{SA} * (1 - \epsilon \Delta T) \tag{32}$$

Where P_{th} is specific power due to thermal effects, and $\triangle\ T$ is the change in temperature and the input parameters.

3. Long-term solar array performance

The power generation capability of an SSA is influenced by multiple interdependent factors, including seasonal variations in solar irradiance, orbital mechanics, degradation effects, and thermal cycling. Ensuring stable power generation over an extended mission duration is crucial for operational reliability.

3.1. Solar power under seasonal variations

The seasonal variation in solar power generation is primarily attributed to the Earth's axial tilt and changes in the Sun-spacecraft orientation over the year. These effects lead to fluctuations in solar exposure, particularly during the summer and winter solstices. Fig. 6 illustrates the solar power output over different months, showing a peak

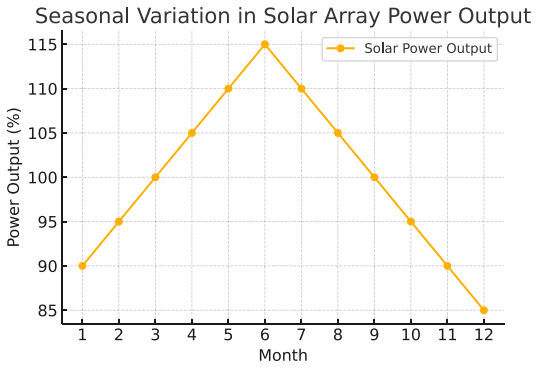

Fig. 6. Seasonal variation in solar array power output over a one-year period.

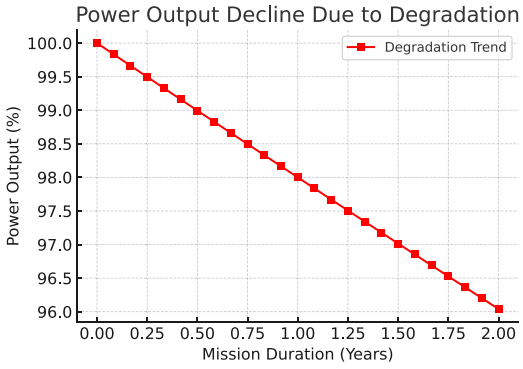

Fig. 7. Power output decline due to radiation-induced degradation over a two-year period.

around the summer solstice and a minimum during the winter solstice. The key observations are that the peak power output occurs during the summer solstice due to maximum solar exposure. Moreover, a power reduction of approximately **10-15%** is observed during the winter solstice due to increased eclipse duration. The power fluctuations align with orbital variations, confirming the dependence of SSA performance on seasonal solar angles.

3.2. Long-term degradation effects

SSA experiences efficiency losses over time due to radiation damage, atomic oxygen erosion, and thermal stress. This degradation follows an exponential decay model, which is mathematically expressed as:

$$P_{EOL} = P_{BOL} \times (1 - D_{TJ})^{t}, \tag{33}$$

where P_{EOL} and P_{BOL} and the end-of-life and the beginning-of-life power output, respectively. D_{TJ} is the annual degradation coefficient (assumed to be 2% for GaAs solar cells), while is the mission duration in years.

As depicted in Fig. 7, the power loss follows a cumulative pattern with a **4% reduction** in power output observed after one year. The total **8% loss** is recorded after two years, requiring sufficient power margins in spacecraft design.

3.3. Impact of thermal cycling

Thermal fluctuations in LEO significantly impact SSA performance. The spacecraft undergoes rapid heating and cooling cycles as it transitions between sunlight and eclipse phases. The temperature-dependent efficiency variation of the GaAs solar cells is described by:

$$\eta(T) = \eta_{ref} \times \left(1 + \alpha_T \times (T - T_{ref})\right), \tag{34}$$

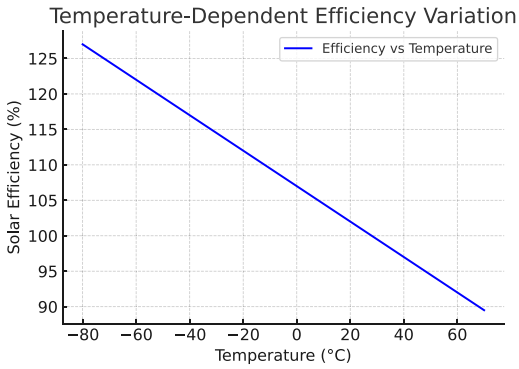

Fig. 8. Temperature-dependent efficiency variation due to thermal cycling in LEO.

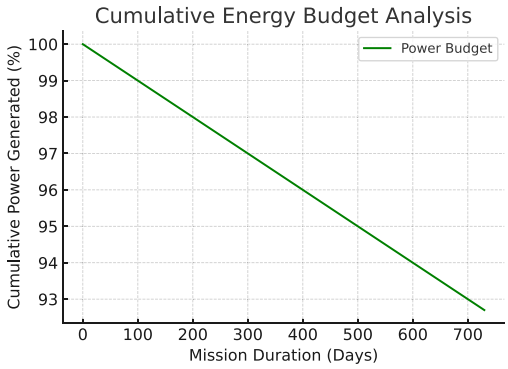

Fig. 9. Cumulative energy budget analysis over the mission lifetime.

where $\eta(T)$ is the solar cell efficiency at temperature T, while η_{ref} is the reference efficiency at $T_{ref} = 28$ °C. α_T is the temperature coefficient (-0.0025 per °C). T is the instantaneous SSA temperature.

Major findings from Fig. 8 are that the temperature fluctuations range from −80 °C (eclipse) to +70 °C (direct sunlight). A temporary **5%–7% reduction** in power output occurs at peak temperatures due to increased internal resistance. The cooling effect during eclipse phases restores efficiency, but repeated thermal cycling introduces structural fatigue in solar cells.

3.4. Energy budget and power margin considerations

A comprehensive power budget analysis must account for seasonal variations, degradation effects, and thermal cycling losses. To maintain operational feasibility, a safety margin of 15%–20% above nominal power requirements is recommended.

$$P_{required} = P_{nominal} \times (1 + M), \tag{35}$$

where $P_{required}$ is the total power generation requirement. $P_{nominal}$ is the nominal mission power consumption. M is the power margin factor (15%–20%).

The designed SSA ensures stable power generation across all mission phases, as depicted in Fig. 9. The power margin compensates for cumulative efficiency losses. Energy storage systems successfully mitigate power fluctuations during eclipse phases.

4. Mission cyclogram design with power budget calculations

Spacecraft mission cyclogram design is a crucial aspect of maximizing the spacecraft efficiency while ensuring optimal power allocation during the worst-case scenario. This cyclogram involves analysing various operational scenarios, e.g., different orbital positions, payload activities, and communication requirements. Therefore it is required to determine a comprehensive schedule that minimizes conflicts and maximizes resource utilization. This process can be achieved by determining the overall energy consumption of the spacecraft during its mission lifespan.

This calculation involves accounting for the solar energy availability and the load profile of each subsystem and payload, considering factors e.g., spacecraft orientation, SSA temperature, and shadowing effect. For worst-case conditions, energy budget analysis requires to consideration of various margin factors, e.g.:

- EOL worst-case SSA degradation.
- Summer solstice intensity.
- Battery has one shorted cell.
- SSA high temperature.
- Spacecraft load profile with payload operation.
- SSA off-point angle variation.
- SSA clamped to battery voltage after the eclipse.

4.1. Spacecraft platform description

The underlying spacecraft platform is the LEOS platform, which houses various components and systems necessary for ensuring reliable and efficient operations of spacecraft in orbit [23]. Technical specifications of LEOS platform versions 50MR, 50HR, and 100HR are given in Table 4 [24,25]. The LEOS platform is assumed to operate in a specific space mission with a lifetime of up to two years. The spacecraft orbit around the Earth is circular at 668 km altitude, and the orbit inclination is 63°. The degradation coefficients, such as D_{TJ}, are altitude-dependent because the radiation environment varies with orbital altitude. In this study, the degradation coefficients are calculated for the specific altitude of 668 km, which is representative of the spacecraft's orbit. For missions at different altitudes, the degradation coefficients would need to be adjusted based on the specific radiation environment".

Moreover, the LEOS platform provides support for the spacecraft payload, power generation and distribution systems, communication subsystems, thermal control mechanisms, attitude control and propulsion systems. In this context, the primary power supply system (PPSS) must provide power with a bus voltage of 28.5 V as well the power control. The power control distribution unit (PCDU) is switched off when the spacecraft is inside the launch vehicle. Then PCDU is switched on automatically after separating the spacecraft from the launch vehicle. The PCDU operates continuously for the whole spacecraft lifetime according to the duty cycle and power consumption specified by the spacecraft operational modes' power dissipation given in Table 1 [24, 25].

The output power value delivered by every solar panel should satisfy the load requirements at the mission EOL, at the worst case of illumination with the SSA surface facing solar irradiance. This case might happen during the summer solstice with the normal line oriented to the SSA surface).

4.2. PCDU design interface

The PCDU design interface serves as the central point for managing, controlling, and distributing power through the spacecraft. A well-designed PCDU interface ensures efficient utilization of available power resources while offering flexibility to cater to diverse mission requirements. The interface design must accommodate the integration of various equipment like solar panels, batteries, and other power management devices seamlessly. Additionally, it should provide comprehensive monitoring and control capabilities to enable operators to regulate voltage levels and protect against potential faults or failures in real time. The design should also consider factors such as weight, size limitations, thermal management, electromagnetic interference mitigation, reliability, and redundancy [26].

Table 1
Spacecraft operational modes power dissipation [23].

Spacecraft operational mode	Designed o/p power	PCDU power dissipation
Idle	5 W	≤0.5 W
Sun pointing	15.5 W	≤0.5 W
Imaging	70 W	≤0.5 W
Data transmission	50 W	≤0.5 W

Table 2
Inter-connection between the strings of the body-mounted solar panels and the batteries module.

	LiFePO4 (B1)	LiFePO4 (B2)	LiFePO4 (B3)
Panel (-Y)	2	2	2
Panel (+X)	2	–	–
Panel (-Z)	–	2	–
Panel (-X)	–	–	2

Table 3
Storage battery module technical characteristics [23].

Parameter	Value
Number of series connected cells	7 series LiFePO4 cells
end of charge Module voltage	25.2 [V]
Constant operating voltage	23 [V]
Cell capacity	2.5 [Ah]
Maximum allowed charging current	2.5 A = 1C recommend 1/2 C
Depth of Discharge (DoD) Voltage at 18% (DoD) discharge Voltage at 30% (DoD) discharge	18% 22.4 [V] 21.7 [V]
Cut-off voltage (70% (DoD) discharged)	21 [V]
Maximum discharge current	7.5 [A]

In this work, PCDU controls the operation of 3 parallel identical Lithium iron phosphate (LiFePO4) battery modules. The battery module has a 7.5 [Ah] capacity, corresponding to 157 [Wh] energy. The electric characteristics of the battery module are given in Table 3 [23], which provides the technical characteristics of the storage battery module as documented in the referenced source. To ensure its charging capabilities, a hardware interconnection mechanism is designed for the energy storage module as shown in Table 2. This hardware interconnection mechanism ensures the charging of the battery module in all illumination conditions and spacecraft orientation during the flight in orbit.

4.3. Solar array specifications

In this work, the SSA design is proposed to be a 6/2/2/2 configuration according to the designed optimum Sun vector. In total, these strings will be mounted on the four panels of the bus surface of the LEOS platform structure. The panel consists of a string of 12 cells in series [22,23]. The spacecraft electrical design requirements and the SSA characteristics are illustrated in Table 5 [2,23].

4.4. Spacecraft orbital motion

Also, a simplified model of spacecraft orbital motion is used to estimate the SSA illumination and to determine the most effective sun-pointing vector for the sun-tracking flight mode [1,4]. For instance, for a spacecraft operating in a circular orbit, the orbital illumination parameters are characterized by an angle α of the spacecraft orbital plane concerning the Sun, as shown in Fig. 2.

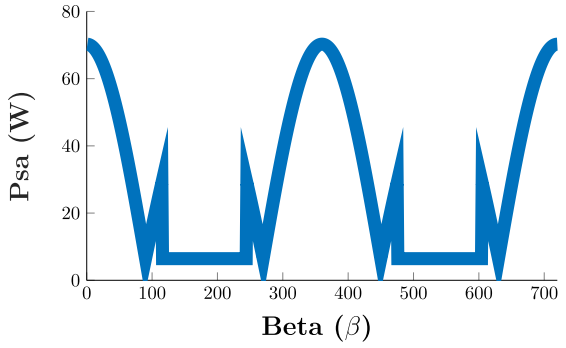

Fig. 10. Solar array specific power VS true anomaly β, i.e., the angle between the direction to the Sun and the noon line.

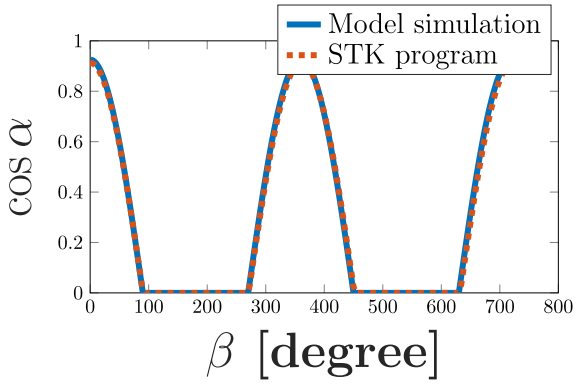

Fig. 11. Illumination coefficient, $\cos\alpha$, Model simulation VS calculated by STK program. Beta (β) is the angle between the direction to the Sun and the noon line (satellite in orbit position).

5. Validation of the solar array model

The proposed SSA model is validated to ensure the accuracy and reliability of simulations of SSA performance under specific conditions. Therefore, extensive testing and analysis are conducted using real data obtained from the existing SSA platform. For instance, this validation includes measuring various parameters, e.g., current–voltage characteristics, temperature coefficients, and spectral responses. Additionally, sophisticated software tools are utilized to simulate different scenarios and compare the results with actual measurements. Afterwards, any discrepancies between the modelled and observed data can be addressed, leading to improved models to provide more accurate predictions for designing optimal solar power systems.

Fig. 11 presents the variation of the illumination coefficient $\cos f_0 \cos\alpha$ as a function of the true anomaly β, where α represents the angle between the direction to the Sun and the normal to the SSA surface. This coefficient is critical in evaluating the effective solar irradiance incident on the solar arrays. The results are shown for both a model simulation and calculations performed using the STK software, enabling a direct comparison. Key insights of these results are the following:

1. Illumination Cycles: The plot exhibits a periodic pattern where the illumination coefficient $\cos f_0 \cos\alpha$ reaches a maximum of 1 during direct sunlight phases. Thus it indicates full exposure of the solar arrays to solar irradiance. During eclipse phases, $\cos f_0 \cos\alpha$ drops to zero, corresponding to periods of no solar illumination.
2. Validation with STK: The close alignment between the model-simulated results and STK-calculated values highlights the accuracy and reliability of the developed model. The near-perfect

match between the two datasets confirms that the proposed simulation methodology effectively captures the illumination dynamics of SSA in LEO orbit.

3. Shadow Factor: The figure also reflects the role of shadow effects, emphasizing transitions between illuminated and shadowed states. This transition is critical for optimizing power generation and understanding thermal conditions.
4. Contribution: The figure provides strong evidence of the capability of the proposed model to replicate real orbital conditions with high fidelity. By incorporating $\cos f_0 \cos \alpha$, a key parameter for energy generation, this visualization contributes to refining spacecraft design and operation, ensuring efficient energy utilization in LEO.

The comparison between the model and STK results reinforces the work contribution to validating and advancing spacecraft illumination modelling, with applications in mission planning and SSA optimization.

The validation process of the proposed SSA model encompasses a series of meticulous tests and analyses using real data derived from an existing SSA platform. These validation efforts aim to ensure the accuracy, reliability, and fidelity of the simulations conducted on the SSA performance under specific operational conditions. Discrepancies can be identified and addressed by comparing the simulated results with actual measurements, ultimately enhancing the model predictive capabilities for designing optimized solar power systems for space missions.

6. Results and discussion

In this work, we developed a power generation model for a SSA for the LEO spacecraft. This model simulates the real capabilities of the designed SSA and the power generated under the whole operating conditions including the influence of thermal effects. The subsequent discussion delves into the SSA behaviour for one day during 15 revolutions around the Earth, providing insights into its performance under different circumstances.

Notably, our research investigates a spectrum of parameters affecting SSA performance, encompassing orbit altitude, orientation, and atmospheric conditions. These factors collectively contribute to the efficiency of power generation, and our study rigorously examines their impact on the SSA, thereby addressing critical aspects often overlooked in existing literature. Through our meticulous research and analysis, we not only establish the efficiency and feasibility of our SSA power generation model but also contribute novel insights that distinguish our work from existing studies. The results demonstrate the successful simulation of SSA operation, showcasing its ability to convert sunlight into electric energy with an impressive conversion rate. The application of a high-efficiency model ensures an optimal power profile, guaranteeing uninterrupted operation under various conditions.

6.1. Generated solar power

Comparing the model predictions for the power generated by the SSA with actual power output measurements further contributes to validation as shown in Fig. 12. This involves analysing the relationship between solar irradiance, Sun angles, and SSA efficiency. Discrepancies in power generation estimates are meticulously evaluated to refine the model predictive capabilities.

Fig. 12 illustrates the variation in the generated solar power over time, plotted in seconds. The periodic nature of the solar power output reflects the spacecraft orbit, where it alternates between illuminated and eclipse phases. The key observations from these results are the following:

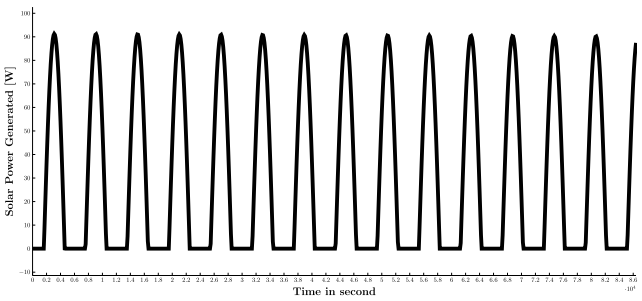

Fig. 12. Generated solar power.

1. Periodic Solar Power Generation: The plot shows a repeating pattern of power generation. During sunlight phases, the solar arrays operate at peak efficiency, generating maximum power. In eclipse phases, solar power generation drops to zero due to the absence of solar irradiance.
2. Peak Performance: The consistent magnitude of the power generated during illuminated phases indicates that the solar arrays are effectively capturing solar energy. This reflects the system ability to optimize energy capture based on Sun angles and solar irradiance.
3. Eclipse Impact: The sharp transitions between peak and zero power output highlight the spacecraft movement between the illuminated and shadowed regions of its orbit, reinforcing the importance of energy storage systems (batteries) to maintain a continuous power supply.
4. Model Validation: The figure supports the validation of the predictive model developed in this study by comparing the simulated power output with actual measurements from real-time telemetry data. The high consistency between model predictions and observed power output demonstrates the accuracy of the model in accounting for solar irradiance, Sun angles, and the efficiency of the solar arrays.

These observations highlight the following contributions:

1. Improved Predictive Accuracy: The ability to predict solar power generation with high accuracy ensures optimal design and operation of the spacecraft's energy system, contributing to mission reliability and efficiency.
2. SA Performance Evaluation: The figure highlights the efficiency of the solar arrays in converting solar energy to electrical power. Any discrepancies between predicted and observed power outputs can be used to refine the model, improving its predictive capabilities.
3. Energy Management Insights: The periodic power profile provides insights into energy availability, enabling efficient scheduling of power-intensive operations during illuminated phases while ensuring adequate battery charge during eclipse phases.
4. Validation Methodology: By integrating real-time telemetry data, the study validates the relationship between solar irradiance, Sun angles, and SSA efficiency, ensuring the reliability of the energy system design under real orbital conditions.

This figure emphasizes the SSA robustness and the accuracy of the predictive model, thus it contributes to the development of advanced energy systems for spacecraft operating in LEO environments.

6.2. Average solar power

The proposed SSA model shortcomings can be addressed through meticulous comparison, analysis, and adjustment, improving and accurately representing the SSA behaviour. This iterative validation process

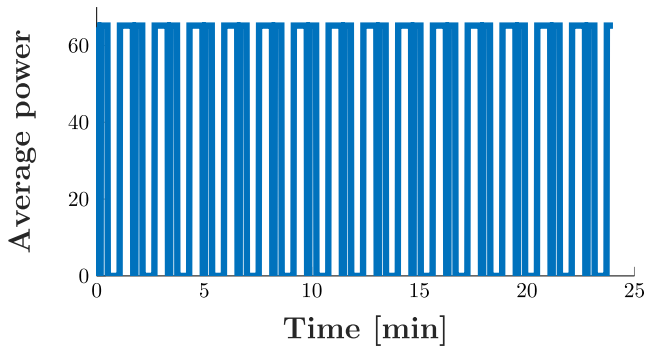

Fig. 13. Average solar power generated Vs. time [min] [23,37,38].

aims to achieve a model that reliably predicts SSA performance, thus it allows for designing efficient and optimized power systems for space missions. Ultimately, this validation process enhances the overall success and reliability of micro-spacecraft missions reliant on solar power generation.

In this work, the obtained SSA power model was validated by comparing the $\cos(\alpha)$ calculated by the designed MATLAB program with $\cos(\alpha)$ generated by STK software as shown in Fig. 11. The interesting finding is that they are almost the same.

The simulation results are validated by comparing our simulation results with the proposed spacecraft telemetry as shown in Fig. 13. These figures indicate the same results of the proposed model with the spacecraft telemetry [23,37,38].

Fig. 13 depicts the variation in the average solar power generated by the spacecraft's SSA over time, measured in seconds. The figure highlights the cyclic nature of power generation in LEO Orbit, as influenced by the spacecraft orbital dynamics and its exposure to solar radiation. Key observations from these results are as follows:

1. Periodic Power Generation: The plot shows a repeating pattern of power generation, with intervals of high average power corresponding to the sunlight phases of the orbit and intervals of zero power during eclipse phases. This periodicity reflects the spacecraft's alternating exposure to sunlight and Earth's shadow as it traverses its orbit.
2. Stability During Illumination: The flat-topped peaks indicate a consistent average solar power output during illuminated periods, demonstrating the solar array's ability to maintain stable energy generation when fully exposed to sunlight.
3. Eclipse Impact: The troughs, where the power drops to zero, represent the eclipse phases where the spacecraft is shielded from solar irradiance. These periods are critical for assessing energy storage and power management strategies to ensure uninterrupted spacecraft operation.
4. Validation of the Model: The periodic nature of the average solar power generation aligns with theoretical predictions and validates the computational model developed in this study. The use of real-time telemetry data ensures the reliability and accuracy of the simulated results, particularly in capturing the spacecraft's real orbital behaviour.
5. Contribution: This figure underscores the importance of modelling and simulating solar power generation dynamics for spacecraft operating in LEO. By accurately predicting power output over time, the study contributes to optimizing energy system designs, ensuring reliable operation, and supporting mission planning.

The visualization effectively demonstrates the robustness of the SSA design and the model's predictive capabilities, providing a foundation for improving spacecraft energy systems in future missions.

6.3. Sun angle calculation

The validation process also focuses on accurately calculating the Sun angles. The angles at which sunlight strikes the SSA directly affect its power generation, as shown in Fig. 15. The accuracy of Sun angle predictions can be assessed by comparing the calculated Sun angles with those obtained from spacecraft positioning data.

Fig. 15 depicts the calculated variations of Sun angles over time, measured in seconds, as a function of the spacecraft's orbital dynamics. The figure illustrates multiple components of angle calculations, including solar incidence angle and angular conversions, which are critical for assessing SSA performance and power generation. The key observations from these results are the following:

1. Sun Incidence Angle on Solar Array (Green Dashed Line): The Sun incidence angle represents the angle at which sunlight strikes the surface of the solar arrays. This parameter directly impacts the efficiency of solar energy conversion. The periodic variation reflects the orbital motion, with the angle increasing during shadow phases and decreasing during illuminated phases.
2. Angle Conversion Metrics (Black, Blue, and Orange Lines): These angular conversions represent intermediary steps in the calculation of Sun angles, accounting for spacecraft orientation, orbital position, and solar geometry. The variations in these values provide critical insights into the spacecraft's relative orientation to the Sun.
3. Cyclic Patterns: The cyclic nature of the angular metrics highlights the periodic changes in the spacecraft's orientation relative to the Sun and Earth, characteristic of LEO dynamics. The sharp peaks and troughs align with transitions between illuminated and shadowed regions of the orbit.
4. Model Validation: The close agreement between the calculated Sun angles and those derived from spacecraft positioning data validates the model accuracy. This highlights the capability of the model to capture real-world orbital behaviours and their impact on SSA performance.

These observations highlight the following contributions:

1. Sun Angle Prediction Accuracy: The accurate calculation of Sun angles is fundamental to optimizing the design and operation of solar arrays. This figure validates the model's ability to predict Sun angles precisely, ensuring reliable energy generation.
2. Impact on Solar Array Performance: The relationship between Sun angles and SSA performance emphasizes the importance of proper orientation for maximizing solar power output. The figure supports this by demonstrating the periodic alignment of the SSA with optimal angles during illuminated phases.
3. Validation with Spacecraft Data: By comparing model predictions with spacecraft positioning data, the study ensures the reliability of the angle calculation method, enhancing confidence in its integration into SSA energy models.
4. Energy Management Optimization: Understanding the Sun angles allows for better scheduling of spacecraft operations, ensuring efficient use of solar energy and minimizing reliance on stored energy during eclipse phases. This figure underscores the critical role of accurate Sun angle calculations in predicting SSA performance and optimizing spacecraft energy systems, contributing to the overall reliability of the spacecraft in LEO environments.

6.4. SSA operating temperature

To underscore the novelty of our results, Fig. 14 presents the SSA operating temperature over time, providing a dynamic visualization of its performance under different thermal conditions. Fig. 14 presents

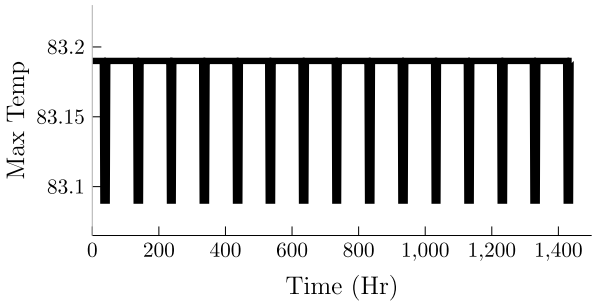

Fig. 14. Solar array temperature over time: dynamic visualization of its performance under different thermal conditions.

the time-dependent variation in SSA temperature, which highlights the dynamic thermal response under varying orbital conditions. The graph illustrates periodic fluctuations in temperature, corresponding to the spacecraft transitions between sunlight (illumination) and shadow (eclipse) phases within its orbit.

The observations from these results are the following:

1. Temperature Cycles: The repeated peaks and troughs reflect SSA exposure to direct solar radiation during daylight phases and the cooling effect during eclipses. This periodic behaviour is intrinsic to the orbital environment, where thermal loads alternate with shadow cooling.
2. Thermal Behaviour: The magnitude and consistency of the temperature variation demonstrate the ability of the thermal design to withstand rapid heating and cooling cycles while maintaining structural and operational stability.
3. Performance Insight: The data validate the thermal modelling environment developed in this study, which incorporates real-time telemetry data to simulate SSA performance under realistic space conditions. The precise alignment of modelled and measured temperatures reinforces the accuracy and reliability of the predictive thermal model.

This visualization underscores the robustness of the spacecraft thermal design and its ability to effectively manage dynamic thermal conditions. It also validates the methodology for integrating telemetry data into thermal simulations, which contributes to the advancement of spacecraft thermal modelling and design in LEO environments.

6.5. Average orbital power

In the initial design phase of the spacecraft and during the operation of the SSA in orbit, it is helpful to know the power over all possible orbits. To determine the available power over all possible β. Fig. 10 further illustrates the total power generated by the Solar Array, considering external factors and thermal effects. Thus, it will reflect the real capabilities of the SSA to execute the designed mission requirements. Crucially, the introduced parameter K_{th}, which represents the ratio of specific power due to thermal effects to the specific power of SSA, is calculated as 0.9935, based on the ratio of the specific power due to thermal effects (P_{th}) to the specific power of the solar array (P_{SA}). This value is derived from the thermal model and validated using real-time telemetry data from the LEOS-50 platform.[2]

$$\mathrm{K_{th}} = \mathrm{P}_{th}/\mathrm{P}_{SA} = 0.9935 \tag{36}$$

[2] To ensure the accuracy of the value 0.9935, it is validated using real-time telemetry data from the LEOS-50 platform. The thermal model's predictions are compared with actual measurements of the solar array's power output under varying thermal conditions, demonstrating good agreement between the model and the observed data.

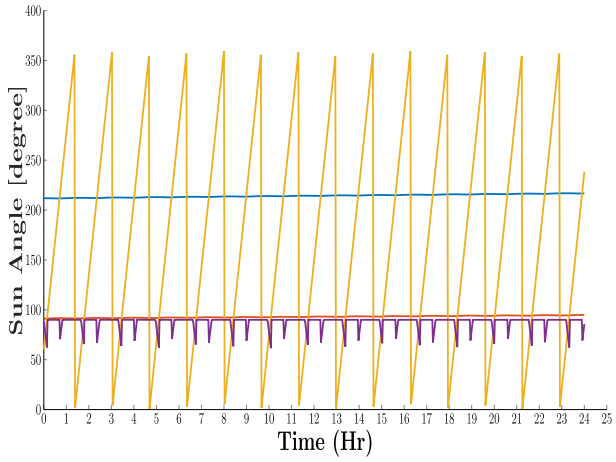

Fig. 15. Sun angle.

This quantification emphasizes the precise control and efficiency achieved in mitigating thermal impacts on power generation. In summary, our study not only establishes the efficacy of our SSA power generation model but also introduces novel parameters and insights that contribute significantly to the current body of knowledge. Our results showcase advancements over existing studies, particularly in the accurate simulation of SSA operation and the quantification of thermal effects through the innovative Kth parameter.

Fig. 10 illustrates the variation of the specific power generated as a function of the true anomaly (β), which represents the angular position of the spacecraft in its orbit relative to the Sun. The plot captures the dynamic behaviour of the SSA power generation in response to varying illumination conditions in LEO orbit.

The key observations from these results are as follows:

1. Cyclic Behaviour: The figure reveals a clear periodic pattern in the specific power output, with peaks corresponding to periods of maximum solar exposure during the sunlight phases of the orbit. The sharp drops to near-zero power indicate the eclipse phases, where the SSA is in the Earth shadow and receives no direct solar irradiance.
2. Orbital Effects: The variation in β reflects the spacecraft relative position to the Sun, emphasizing the dependency of power generation on the angle between the SSA and the Sun. This demonstrates the importance of orientation and solar tracking to maximize energy capture.
3. Performance Validation: The periodic power output aligns with the theoretical predictions of the SSA performance under modelled conditions. This validates the modelling approach developed in the study, which uses real-time telemetry data to accurately simulate and predict power generation.
4. Contribution: The analysis highlights the effectiveness of the SSA design in maintaining a consistent and predictable power profile, which is crucial for ensuring the uninterrupted operation of onboard systems. The integration of real-time telemetry data into the model provides critical insight into optimizing power generation in dynamic orbital environments.

This figure is a key contribution to the study as it demonstrates the practical application of the developed model in accurately predicting SSA performance, thereby supporting the advancement of energy system designs for spacecraft in LEO.

6.6. Sun angle incident on the SSA

Ensuring that the Sun angle calculations only consider the portion of the Sun illumination that directly impacts the SSA is essential.

This validation step excludes any angles that correspond to shading or obstruction from other spacecraft components, as shown in Fig. 16. By validating this aspect, the model predictions align with the practical realities of SSA exposure to sunlight.

Fig. 16 illustrates the Sun angle incident on the SSA over time, measured in seconds. The plot specifically highlights the angular position of sunlight directly impacting the solar array, excluding any effects from shading or obstructions caused by other spacecraft components.

The key observations from these results are the following:

1. Periodic Sun Angle Variation: The Sun angle exhibits a periodic pattern, reflecting the spacecraft's movement through its orbit. During illuminated phases, the angle is optimized for solar energy capture, while during eclipse phases, the angle increases due to the absence of direct solar exposure.
2. Sharp Transitions: The sharp transitions between low and high Sun angles correspond to the transitions between the illuminated (daylight) and eclipse (shadow) portions of the orbit. These transitions align with the spacecraft orbital motion in LEO.
3. Exclusion of Obstructions: The figure ensures that only the portion of the sun's illumination directly incident on the SSA is considered in the model. This eliminates any angular components associated with shading or obstructions, ensuring the accuracy of the calculated Sun angles.
4. Model Validation: The alignment between the predicted Sun angles and observed values demonstrates the reliability of the model in capturing the practical realities of SSA exposure to sunlight. The exclusion of obstructed angles further enhances the precision of the model.

These observations highlight the following contributions:

1. Refinement of Sun Angle Calculations: The focus on direct solar incidence ensures that the model accurately represents the actual exposure of the solar arrays, leading to more precise predictions of solar power generation.
2. Enhanced Solar Array Efficiency: By isolating the useable portion of sunlight, the figure supports the optimization of SSA orientation and design to maximize energy capture during illuminated phases.
3. Validation of Practical Application: The figure validates the model's applicability by aligning its predictions with real-world conditions, accounting for factors like orbital motion and structural geometry.
4. Impact on Energy System Design: Accurate Sun angle calculations are critical for optimizing spacecraft energy systems. This figure underscores the importance of considering only direct sunlight, ensuring robust performance under operational conditions.

This figure demonstrates the significance of precise Sun angle calculations in predicting SSA performance, contributing to the overall reliability and efficiency of spacecraft energy systems in LEO environments.

The Sun angle, defined as the angle between the normal to the solar array and the Sun direction, exhibits non-periodic behaviour due to several dynamic orbital and external influences:

- Orbital Precession and Perturbations: The spacecraft orbit undergoes gravitational perturbations due to Earth's equatorial bulge, resulting in a slow but continuous precession of the orbital plane. This causes a gradual shift in the Sun angle over time, preventing strict periodicity in the short term.
- Sun-Synchronous Orbit Effects: In a Sun-synchronous orbit, the Sun angle changes gradually due to Earth's axial tilt and seasonal variations, contributing to long-term fluctuations.

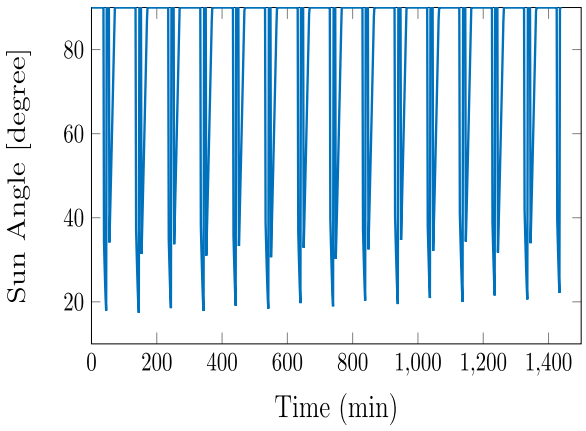

Fig. 16. Sun angle incident on the SSA.

- Eclipse Occurrence and Geometry: The frequency and duration of eclipse periods are influenced by the orbital altitude and inclination, which further modulate the Sun angle irregularly over time.

These factors contribute to the non-periodic nature of the Sun angle over short durations, even though they follow predictable long-term trends.

6.7. SSA temperature panel calculation

Temperature is a critical factor that influences the performance of SSA. The model ability to predict temperature variations across the solar panels is validated against actual thermal measurements as shown in Fig. 17. This step includes assessing how accurately the model accounts for the effects of solar heating, radiative cooling, and other thermal dynamics in space.

The key observations from these results are the following:

1. Periodic Temperature Fluctuations: The temperature profile demonstrates a clear cyclic behaviour. During sunlight phases, the panels heat up due to solar irradiance, while during eclipse phases, the panels cool down as they radiate heat into space. The consistency of these fluctuations reflects the orbital dynamics of the spacecraft.
2. Thermal Stability: The predictable maximum and minimum temperature levels indicate a stable thermal environment for the solar arrays, suggesting that the thermal design effectively mitigates extreme temperature variations.
3. Solar Heating and Radiative Cooling: The periodic heating during illuminated phases and cooling during eclipse phases emphasize the importance of accurately modelling the thermal dynamics affecting the solar panels. These factors directly impact the efficiency and longevity of the solar arrays.
4. Model Validation: The comparison of the predicted temperature variations with actual spacecraft telemetry data validates the accuracy of the thermal model. The model successfully captures the influence of solar heating, radiative cooling, and the spacecraft's thermal design.

These observations highlight the following contributions:

1. Enhanced Thermal Modelling: This figure underscores the model's capability to predict the thermal behaviour of solar panels accurately. By including critical parameters such as solar heating and radiative cooling, the model provides reliable predictions for thermal performance.

2. Design Optimization: The insights from the thermal calculations help refine the SSA design, ensuring it operates efficiently under the harsh thermal conditions of space. The stability of the temperature profile is essential for maintaining the structural and operational integrity of the solar panels.
3. Validation Against Real Data: The close alignment of the model's results with spacecraft telemetry data confirms the robustness and reliability of the thermal model, ensuring its applicability in designing and optimizing solar-powered spacecraft.
4. Iterative Improvement: The identified discrepancies between the model and real-world data allow for iterative refinement of the thermal simulation, leading to increasingly accurate predictions of SSA behaviour and enhanced mission success.

This figure highlights the critical role of thermal modelling in ensuring the efficient operation of solar arrays in LEO environments. By accurately predicting temperature variations, the model contributes to the development of robust and reliable energy systems for space missions. Unlike the Sun angle, solar power output and temperature exhibit a strictly periodic behaviour due to the dominance of the orbital cycle:

- Orbital Illumination Cycle: The spacecraft undergoes a predictable cycle of **daylight and eclipse** every orbit (approximately 90 min in LEO). This ensures that solar power generation follows a strict periodic pattern, rising during sunlight and dropping during the eclipse.
- Thermal Equilibrium Dynamics: The solar array absorbs solar energy during illumination, increasing its temperature, and radiates heat during eclipse, causing cooling. This results in a predictable periodic heating and cooling cycle.
- Power System Regulation: The spacecraft's power management system adjusts the power conversion and battery charging process, stabilizing energy output despite Sun angle fluctuations.

Thus, while the Sun angle follows a non-periodic trajectory, the solar power output and temperature remain strictly periodic due to their dependence on the short-term orbital cycle. This analysis demonstrates that:

- The Sun angle is non-periodic in short-term analysis due to orbital precession, seasonal shifts, and eclipse variations.
- Solar power and temperature remain fully periodic because they are governed by the stable, repetitive orbital cycle.

These findings confirm that while Sun angle fluctuations introduce long-term variations, the primary driver of periodic power and thermal behaviour is the orbit itself. This insight is crucial for designing energy management strategies in Low Earth Orbit missions.

6.8. Impact of performance degradation on solar array output

The obtained results also show the decline in power generation as a result of radiation-induced degradation and temperature effects over the spacecraft's mission lifetime. The predictions of the degradation models are compared with real-time telemetry data from the LEOS-50 platform to validate their accuracy. This comparison demonstrates the ability of the models to capture the long-term behaviour of the solar array under realistic conditions. Therefore, degradation must be taken into account when sizing the solar array and battery system. This includes recommendations for mitigating degradation effects, such as optimizing the array's orientation and incorporating redundancy.

7. Conclusions

In conclusion, modelling SSA power generation for LEO spacecraft is a complex and multidimensional task. The novelty of this (modelling/simulation) approach is to validate the SSA capabilities within the designed mission operation scenarios under external factors. The proposed environment leads to ensuring the SSA outputs and capabilities to perform the mission-designed scenarios before starting the manufacturing process. Thus, it provides a useful tool in designing future SSA of LEO spacecraft. The mathematical model obtained allows to guarantee of the execution of the proposed power budget throughout the spacecraft's life cycle.

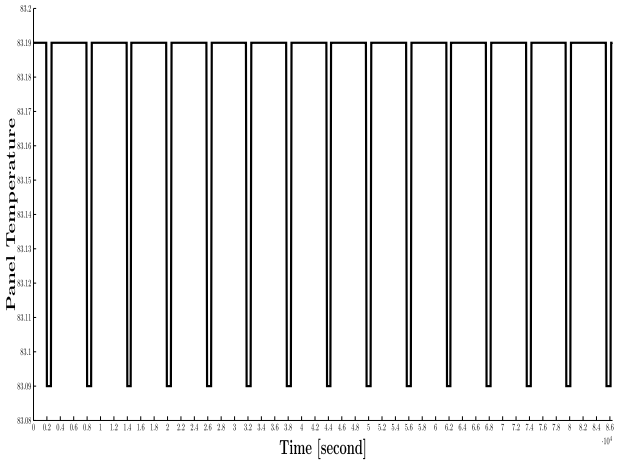

Fig. 17. Panel Temperature calculation.

The results were validated by the STK program using the LEOS-50 commercial platform telemetry analysis. The interesting point is that the power capability of the commercial platform of LEOS-50 is suitable for the proposed new spacecraft design scenario load profile. This study can contribute to the development of efficient and reliable power subsystems, which are essential for the success of spacecraft missions.

Further potential research directions in the SSA model incorporate a machine learning algorithm utilizing the available real-time data from different platforms. Moreover, integrating the attitude control system within the SSA might be effective in maximizing energy production.

CRediT authorship contribution statement

Ahmed Mokhtar: Writing – original draft, Visualization, Software, Resources, Methodology, Investigation, Formal analysis, Data curation, Conceptualization. **Mohamed Ibrahim:** Writing – review & editing, Writing – original draft, Visualization, Investigation, Formal analysis. **Mohamed E. Hanafy:** Writing – review & editing, Supervision, Project administration, Investigation, Formal analysis, Data curation. **Fawzy H. Amer ElTohamy:** Visualization, Supervision, Investigation, Formal analysis. **Yehia Z. Elhalwagy:** Supervision, Project administration.

Declaration of competing interest

The authors declare that they have no known competing financial interests or personal relationships that could have appeared to influence the work reported in this paper.

Appendix

A.1. Supplemental tables

See Tables 4–6.

Table 4
Technical specifications of LEOS platform versions: 50MR, 50HR, and 100HR.

Parameter	LEOS-50MR	LEOS-50HR	LEOS-100HR
Payload volume	530 × 530 × 200 mm^3 50U	530 × 530 × 340 mm^3 75U	530 × 530 × 620 mm^3 150U
Payload mass	10–15 kg	15–30 kg	30–70 kg
Payload power for 10:30 h 505 km Sun synchronous orbit @ 100% Nadir Pointing + 20 min/day transmit	250 W peak for 10 min per orbit or 25 W av. for 100 min per orbit	250 W peak for 10 min per orbit or 25 W av. for 100 min per orbit	300 W peak for 20 min per orbit or 60 W av. for 100 min per orbit
Platform design lifetime	5 years	5 years	5 years
Heritage	KR1 (2015), KR1B (2016) NExSat	Lagari	10x LEOS-100 for India

Table 5
Configuration of the body-mounted solar panels and the solar cell electrical parameters.

Type of solar cell	Gallium Arsenide triple junction (GaAs)
Number of series cells	12 cells
Manufacturer and cell category	AZUR-space 3 J cell with efficiency 30%
Open circuit voltage of solar cell (1367 W/m2, 28 °C)	2.616 [V]
Short circuit current of solar cell (1367 W/m2, 28 °C)	0.519 [A]
V_m Maximum power point voltage of solar cell (AM0)	2.345 [V]
I_m Maximum power point current of solar cell (AM0)	0.503 [A]
P_m Maximum power of solar cell (AM0)	1.18 [W]
Open circuit voltage temperature coefficient	−6.2 [mV/°C]
Short circuit current temperature coefficient	0.35 [mA/°C]
Maximum power point voltage temperature coefficient	−6.3 [mV/°C]
Maximum power point current temperature coefficient	0.27 [mA/°C]
Average power consumption of the spacecraft $P_{daily/avg}$	35 [W]
Solar cell strings distribution on spacecraft panels	Panel (-Y) 6 solar strings Panel (+X) 2 solar strings Panel (-Z) 2 solar strings Panel (-X) 2 solar strings

Table 6
Spacecraft subsystems power consumption.

Subsystem	Operation duration power consumption (watt)	Standby power consumption (watt)
TTC_S	25	3.5
TTC_TLM	7.5	7.5
AOC Prep.1	12.85	0
AOC Prep.2	19.85	0
AOC Imaging	27.1	0
AOC Discharge	22.75	0
AOC standby	0	10.75
AOC orientation to Sun pointing	54.75	0
CDH	10	10
PL Imaging	60	0
PL download	22	0
PL Stand by	0	2
PLCDHS	10	10
TTC_X	80	0
TTC_GPS	5.3	5.3
PS	6	6

References

[1] K. Kwon, S. Min, J. Kim, K. Lee, Framework Development for Efficient Mission-Oriented Satellite System-Level Design, vol. 10, MDPI, Republic of Korea, 2023, p. 228.
[2] M. Varsha, J. Stephen, S. Divya, R. Geetha, Design and development of an electrical power system for a 3U cubesat, Smart Small Satellites: Design, Modelling and Development: Proceedings of the International Conference on Small Satellites, ICSS 2022, Springer, Springer Singapore, 2023, pp. 127–146.
[3] X. Chen, R. Yuan, J. Zhu, C. Liu, J. Li, Q. Li, Conceptual design and orbit-attitude coupled analyses of free-drift solar power satellite, Adv. Space Res. (2023).
[4] P. Fortescue, G. Swinerd, J. Stark, Spacecraft Systems Engineering, John Wiley & Sons, UK, 2011.
[5] B. Parida, S. Iniyan, R. Goic, A review of solar photovoltaic technologies, Renew. Sustain. Energy Rev. 15 (3) (2011) 1625–1636.
[6] S. Sobri, S. Koohi-Kamali, N.A. Rahim, Solar photovoltaic generation forecasting methods: A review, Energy Convers. Manage. 156 (2018) 459–497.
[7] C. Lupangu, R. Bansal, A review of technical issues on the development of solar photovoltaic systems, Renew. Sustain. Energy Rev. 73 (2017) 950–965.
[8] G. Tiwari, R. Mishra, S. Solanki, Photovoltaic modules and their applications: a review on thermal modelling, Appl. Energy 88 (7) (2011) 2287–2304.
[9] H.A. Kazem, M.T. Chaichan, A.H. Al-Waeli, A. Gholami, A systematic review of solar photovoltaic energy systems design modelling, algorithms, and software, Energy Sources A: Recover. Util. Environ. Eff. 44 (3) (2022) 6709–6736.
[10] P. Malaviya, V. Sarvaiya, A. Shah, D. Thakkar, M. Shah, A comprehensive review on space solar power satellite: an idiosyncratic approach, Environ. Sci. Pollut. Res. 29 (28) (2022) 42476–42492.
[11] A.J. Ali, M. Khalily, A. Sattarzadeh, A. Massoud, M.O. Hasna, T. Khattab, O. Yurduseven, R. Tafazolli, Power budgeting of LEO satellites: An electrical power system design for 5G missions, IEEE Access 9 (2021) 113258–113269.
[12] S. Dahbi, A. Aziz, S. Zouggar, M. El Hafyani, O. Morocco, A. Hanafi, M. Karim, I. Latachi, T. Rachidi, Power budget analysis for a LEO polar orbiting nano-satellite, in: 2017 International Conference on Advanced Technologies for Signal and Image Processing, ATSIP, IEEE, 2017, pp. 1–6.
[13] A. Tadanki, E.G. Lightsey, Closing the Power Budget Architecture for a 1U CubeSat Framework, Tech. Rep., Georgia Institute of Technology, 2019.
[14] S.S. Arnold, R. Nuzzaci, A. Gordon-Ross, Energy budgeting for CubeSats with an integrated FPGA, in: 2012 IEEE Aerospace Conference, IEEE, 2012, pp. 1–14.
[15] A. Sirin, Power system analysis of J3 CubeSat and RATEX-J high voltage power supply calibration, 2015.
[16] D.I. Suryanti, S. Ramayanti, M. Mukhayadi, Preliminary power budget analysis for equatorial low earth orbit (LEO) communication satellite, J. Teknol. Dirgant. 19 (1) (2021) 67–78.
[17] O. Popescu, Power budgets for cubesat radios to support ground communications and inter-satellite links, Ieee Access 5 (2017) 12618–12625.
[18] A. Mokhtar, M. Ibrahim, M.E. Hanafy, F.H.A. ElTohamy, W.A. Murtada, Y.Z. Elhalwagy, A reliable spacecraft power supply subsystem based on discrete water cycle multi-objective optimization, Frankl. Open 7 (2024) 100092.
[19] J. Gonzalez-Llorente, A.A. Lidtke, K. Hatanaka, R. Kawauchi, K.-I. Okuyama, Solar module integrated converters as power generator in small spacecrafts: Design and verification approach, Aerospace 6 (5) (2019) 61.
[20] S. Sanchez-Sanjuan, J. Gonzalez-Llorente, R. Hurtado-Velasco, Comparison of the incident solar energy and battery storage in a 3U CubeSat satellite for different orientation scenarios, J. Aerosp. Technol. Manag. 8 (2016) 91–102.
[21] I.F. Acero, J. Diaz, R. Hurtado-Velasco, S. Gonzalez, S. Rincon, J. Rodriguez-Ferreira, J. Gonzalez-Llorente, et al., A method for validating CubeSat satellite EPS through power budget analysis aligned with mission requirements, IEEE Access (2023).
[22] Azurspace web site:, 2025, www.azurspace.com. (Accessed May 2023).
[23] Satellite eoportal Web site:, 2025, www.eoportal.org. (Accessed May 2023).
[24] S. eoportal, Origins: Eoportal satellite web site:, 2021, URL www.eoportal.org/satellite-missions/.
[25] S. eoportal, Origins | eoportal satellite Web site:, 2021, URL www.eoportal.org/satellite-missions/.

[26] K.D.E. Kerrouche, A. Seddjar, N. Khorchef, S.A. Bendoukha, L. Wang, A. Aoudeche, CubeSat project: experience gained and design methodology adopted for a low-cost Electrical Power System, Automatika 63 (4) (2022) 695–717.
[27] A. Shawky, H. Radwan, M. Orabi, M.Z. Youssef, A novel platform for an accurate modeling and precise control of photovoltaic modules with maximum operating efficiency, in: 2015 IEEE Applied Power Electronics Conference and Exposition, APEC, IEEE, 2015, pp. 205–212.
[28] P. Shen, Q. Chen, L. Xu, Electrical characteristics prediction of microsatellite photovoltaic subsystem in orbit, in: 2015 IEEE Energy Conversion Congress and Exposition, ECCE, IEEE, 2015, pp. 3287–3294.
[29] J.P. Grey, I.R. Mann, M.D. Fleischauer, D.G. Elliott, Analytic model for low earth orbit satellite solar power, IEEE Trans. Aerosp. Electron. Syst. 56 (5) (2020) 3349–3359.
[30] M. Yaqoob, A. Lashab, J.C. Vasquez, J.M. Guerrero, M.E. Orchard, A.D. Bintoudi, A comprehensive review on small satellite microgrids, 37, (10) 2022, pp. 12741–12762, http://dx.doi.org/10.1109/TPEL.2022.3175093,
[31] A.Z. Ribah, S. Ramayanti, Power produced analysis of solar arrays in nadir pointing mode for low-earth equatorial micro-satellite conceptual design, in: IOP Conference Series: Earth and Environmental Science, Vol. 284, IOP Publishing, 2019, 012048.
[32] Amosborne, Design considerations for a spacecraft Solar Array, 2024, URL https://www.osborneee.com/spacecraft-solar-array/.
[33] H. Curtis, Solar array drive assemblies (SADAs) on the global market | satsearch blog — blog.satsearch.co, 2025, https://blog.satsearch.co/2022-12-01-solar-array-drive-assemblies-sadas-on-the-global-market. (Accessed 19 March 2025).
[34] Gomspace.com, 2025, https://gomspace.com/UserFiles/Subsystems/flyer/Tracking_solar_panels_v2.pdf. (Accessed 19 March 2025).
[35] A. Porras-Hermoso, J. González-Monge, S. Marín-Coca, E. Roibás-Millán, Optimal sun-tracking law for remote sensing satellites operating under observation constraints, Acta Astronaut. 222 (2024) 95–108.
[36] Solar arrays | MMA space — mmadesignllc.com, 2025, https://mmadesignllc.com/products/solar-arrays. (Accessed 19 March 2025).
[37] Gpm NASA gov data web site:, 2025, https://gpm.nasa.gov. (Accessed September 2022).
[38] Migration data portal Web site:, 2025, www.migrationdataportal.org. (Accessed September 2022).